Sheffield Hallam University

Ga doping of nanocrystalline CdS thin films by electrodeposition method for solar cell application: The influence of dopant precursor concentration

ECHENDU, O.K., WERTA, S.Z., DEJENE, F.B., OJO, A.A. and DHARMADASA, I. <http://orcid.org/0000-0001-7988-669X>

Available from Sheffield Hallam University Research Archive (SHURA) at:

https://shura.shu.ac.uk/23836/

This document is the Accepted Version [AM]

Citation:

Ga doping of nanocrystalline CdS thin films by electrodeposition method for solar cell application: The influence of dopant precursor concentration

O. K. Echendu[*1], S. Z. Werta[1], F. B. Dejene[1], A. A. Ojo[2] and I. M. Dharmadasa[2]

[1]Solar Energy Materials, Sensors and Luminescence Materials Group, Department of Physics, University of the Free State, Qwaqwa Campus, Private bag X13 Phuthaditjhaba, 9866, South Africa.

[2]Electronic Materials and Sensors Group, Materials and Engineering Research Institute, Sheffield Hallam University, S1 1WB, Sheffield, United Kingdom.

[*]Corresponding author's email: oechendu@yahoo.com;   Phone: +27848831818.

Abstract

Ga doping of CdS thin films has been achieved using a simplified cathodic electrodeposition method and with glass/ indium tin oxide (glass/ITO) as a substrate. $CdCl_2$, $Na_2S_2O_3$ and $GaCl_3$ were used as precursors. The Ga-doped and un-doped CdS films obtained were characterized for their structural, optical, luminescence, compositional and morphological properties using state-of-the-art X-ray diffraction (XRD), spectrophotometry, room-temperature photoluminescence (PL), energy dispersive X-ray spectroscopy (EDX) and scanning electron microscopy (SEM), respectively. XRD results show that the presence of Ga ions in the deposition electrolyte and post-deposition annealing promote crystallinity of deposited CdS films, with estimated crystallite sizes of the films in the range (5 – 22) nm after annealing. Optical characterization results show that incorporation of Ga atoms into the crystal lattice of CdS results in increase in energy bandgap of the films, which makes them advantageous for application as window/buffer layers in solar cells. PL results show a single green emission peak whose intensity increases as Ga-content of the films increases. EDX results show a direct relationship between the percentage atomic Ga composition of the CdS:Ga films and the molar concentration of $GaCl_3$ in the deposition electrolyte. SEM images reveal smooth surfaces of doped and un-doped CdS films. However, after annealing, cracks begin to develop in the films grown with electrolytic $GaCl_3$ concentration in excess of 0.004 M, thus indicating a possible threshold in $GaCl_3$ concentration for obtaining device-grade CdS:Ga films. The entire work presents one of the strengths of electrodeposition as a reliable semiconductor growth technique for device application.

Key words: Ga-doping; electrodeposition; dopant; CdS; CdS:Ga; thin film.

1 Introduction

The importance of CdS as a semiconductor material cannot be over emphasized. Over the years, it has proven to be a very important member of the II-VI semiconductor family, playing significant roles in various types of semiconductor devices ranging from thin film transistors [1] to diodes [2], photoresistors [3], piezo transducers [4], luminescence devices [5], non-linear optics [6], solar cells [7] and so on. As a result, it has attracted huge research attention and continues to do so. A range of techniques have also been used to produce CdS both in bulk and thin film forms. These methods include close space sublimation [8], thermal evaporation [9], sputtering [10], spray pyrolysis [11], metal organic chemical vapour deposition [12], pulsed laser deposition [13], molecular beam epitaxy [14], sol-gel [15], chemical bath deposition (CBD) [16] and electrodeposition [17]. With the opening up of renewable energy as a new field of technology in recent times, there has been a renewed interest in the research on CdS with respect to its application in solar cells. To this end, CdS has found an enviable application as a reliable window/buffer material in thin film solar cells based on CuS [18], CdTe [7], Cu(InGa)Se$_2$ (CIGS) [19] and Cu$_2$ZnSnS$_4$ (CZTS) [20].

Attempts have been made to effectively replace CdS as a solar cell window material in recent times, due to its Cd-content, but these have not really succeeded much [21], making CdS still stand out as a reliable material. However, there are still two major issues with the application of CdS as a window/buffer material apart from the fear of Cd toxicity. These are: its high absorption coefficient, which leads to window absorption and therefore limiting the short-circuit current density of solar cells; and its high resistivity which in addition, increases the solar cell series resistance and therefore lowers the fill factor. In both cases, the overall conversion efficiency of the solar cell is adversely affected. To mitigate the effect of high absorption coefficient, the CdS window layer is usually made considerably thin in solar cells, although extremely thin CdS can lead to leakages in the cell and still compromise the fill factor. An alternative approach is alloying and doping with appropriate elements. To address the issue of high resistivity, doping with appropriate donor atoms has been carried out. Such donor atoms can conveniently come from the group III elements of the periodic table. These include, B, Al, Ga, In and Tl [11, 22 - 26].

In the present work, we have carried out Ga doping of CdS thin films using simplified 2-electrode electrodeposition method with indium tin oxide (ITO) as substrate and GaCl$_3$ as source of Ga ions. We have done this for three main reasons. First, Ga doping of CdS thin films using electrodeposition method has not been reported. The very few available reports of Ga doping of CdS involved mainly chemical bath deposition [23, 24], solvothermal method [25] and thermal evaporation [26]. The use of electrodeposition in producing CdS or CdS:Ga is aimed at providing a single industrial production line in the preparation of both CdS window/buffer material and CdTe, CIGS or CZTS absorber material, as a way of simplifying production process and therefore bringing down cost of solar cell production. This becomes important since all three above mentioned absorber materials can also be produced by electrodeposition method for high

efficiency solar cells [19, 27 - 29]. Second, the use of $GaCl_3$ as Ga precursor in producing CdS:Ga has not been explored. The few available reports have employed mainly $Ga(NO_3)_3$ [23 - 25], elemental Ga and Ga_2O_3 [26]. Since we had previously established and reported the electrodeposition of CdS using $CdCl_2$ as Cd precursor [17, 30], we therefore decided to use $GaCl_3$ as source of Ga doping without introducing additional elements into the deposition electrolyte other than those from the Cd and S precursors. Third, ITO has not been employed as substrate for this purpose. The available reports have also employed borofloat glass [23], fluorine-doped tin oxide (FTO) and glass/Mo substrates [24]. The result of the electrodeposition and characterization of Ga-doped CdS thin films on ITO substrates are therefore presented and discussed in the following sections.

2 Experimental details

The electrolytic bath used for this work principally contains aqueous solution of 0.3 M $CdCl_2.H_2O$ (99.9%, Sigma-Aldrich, South Africa) and 0.03 M $Na_2S_2O_3.5H_2O$ (analytical reagent grade, Laboratory Consumables, South Africa) in 400 mL inside a 600 mL beaker. The pH of the electrolyte was maintained at 1.80±0.02. Prior to the deposition of CdS, the electrolyte was heated on magnetic stirrer heater to a temperature of 80±2 °C with moderate stirring, and a cyclic voltammetry taken to study the CdS deposition process. The substrate used for the voltammetry and subsequent deposition was glass/ITO glass, cleaned with acetone, methanol and de-ionized water. From the resulting cyclic voltammogram obtained and presented in fig. 1, the possible cathodic deposition potentials for CdS was identified to lie between 1300 mV and 1700 mV.
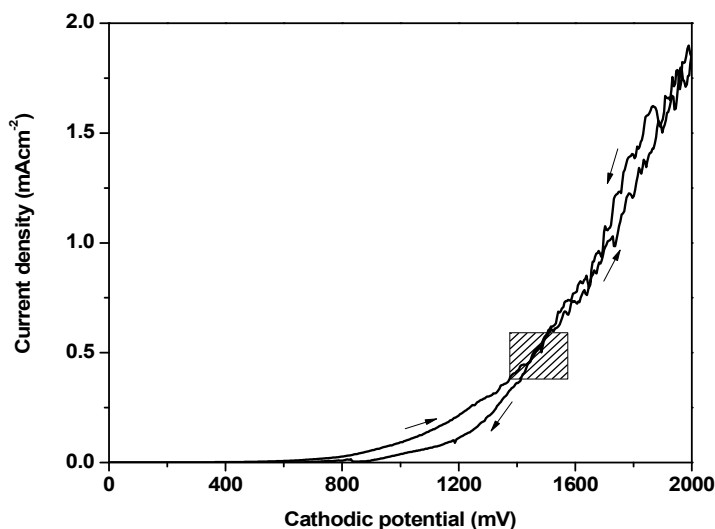

Fig. 1 Cyclic voltammogram of aqueous solution of 0.3 M $CdCl_2$ + 0.03 M $Na_2S_2O_3$ on glass/ITO at pH of 1.8±0.02 and temperature of 80±2 °C.

However, because we had earlier established the cathodic deposition potential of 1450 mV for this electrolytic bath using fluorine-doped tin oxide (FTO) as substrate [17, 30], we decided to settle for 1450 mV (which lies in the neighborhood of the intersection of the forward and reverse sweeps in fig. 1) as the preferred deposition potential in this present work, without further experimentation. At this potential therefore we proceeded to deposit CdS on ITO for 45 minutes at moderate stirring. This sample serves as the un-doped CdS with no Ga^{3+} in the electrolyte. The reason for growing up to 45 minutes is to get sufficiently thick layer for characterization purpose, where the features (especially the X-ray diffraction patterns) will be clearly visible. For solar cell window application, deposition for few minutes is ideal.

In order to proceed with the Ga-doping of CdS, different amounts of $GaCl_3$ (99.99%, DLD Scientific, South Africa) were added into the deposition electrolyte in successive steps. The [Ga]/[Cd] ratios used were 1/100; 1/75; 1/50; 1/25 which correspond to 0.003 M (1%); 0.004 M (1.33%); 0.006 M (2%) and 0.012 M (4%) of $GaCl_3$, respectively. In each case, CdS:Ga film was electrodeposited for 45 minutes. Each CdS sample was divided into two and one part annealed at 400 °C for 20 minute in air atmosphere.

After annealing, all the as-deposited and annealed CdS and CdS:Ga samples were characterized for their structural, optical, luminescence, compositional and morphological properties using X-ray diffraction (XRD), UV-vis spectrophotometry, room temperature photoluminescence (PL), energy dispersive X-ray spectroscopy (EDX) and scanning electron microscopy (SEM). The results of these characterizations are presented and discussed in the next section.

3 Results and discussion

Figure 2 shows the X-ray diffraction patterns of un-doped and Ga-doped CdS thin films in both as-deposited and annealed forms. In as-deposited form, fig. 2(a) shows the CdS films to consist of mixed hexagonal and cubic phases, indexed by the JCPDS reference file numbers 01-075-1545 for hexagonal CdS and 00-021-0829 for cubic CdS. The un-doped film with 0.0 M of Ga in the deposition electrolyte tends to be amorphous or weakly crystalline, with no clearly visible diffraction peaks. The positions where the peaks should appear are defined by weak humps. The only visible peaks are those from the underlying ITO substrate. We attribute this amorphous nature to the effect of the ITO substrate used, as we had previously obtained very crystalline CdS on FTO substrate under the same conditions used in the present work [17, 30]. The effect of the presence of Ga in the electrolyte in the form of $GaCl_3$ is very evident in the appearance of clearly defined diffraction peaks for all the films with Ga concentration from 0.003 M to 0.012 M. Therefore, the presence of Ga promotes the electrocrystallization of CdS by the incorporation of Ga into the crystal lattice of CdS, with the cubic CdS phase taking dominance over the hexagonal phase in the as-deposited form. This is evident in the improvement of intensity of the (200) peak of the cubic phase, as well as narrowing of the full width at half maximum (FWHM)

and the corresponding increase in crystallite size, as can be seen in Table 1. The crystallite size and other crystallographic parameters were estimated from Eqs. (1) – (4).

$$D = \frac{0.94\lambda}{\beta cos\theta} \qquad (1)$$

$$d_{hkl} = \frac{n\lambda}{2sin\theta} \qquad (2)$$

$$\frac{1}{d_{hkl}^2} = \left[\frac{4}{3}(h^2 + k^2 + hk) + l^2\left(\frac{a}{c}\right)^2\right]\frac{1}{a^2} \qquad (3)$$

$$d_{hkl} = \frac{a}{\sqrt{h^2 + k^2 + l^2}} \qquad (4)$$

Where D is the crystallite size, λ is X-ray wavelength, which is 1.54 Å, β is FWHM of the diffraction peaks, θ is the diffraction angle, n is an integer and h,k,l are the miller indices. Eq. (3) is for hexagonal structure while Eq. (4) is for cubic structure.
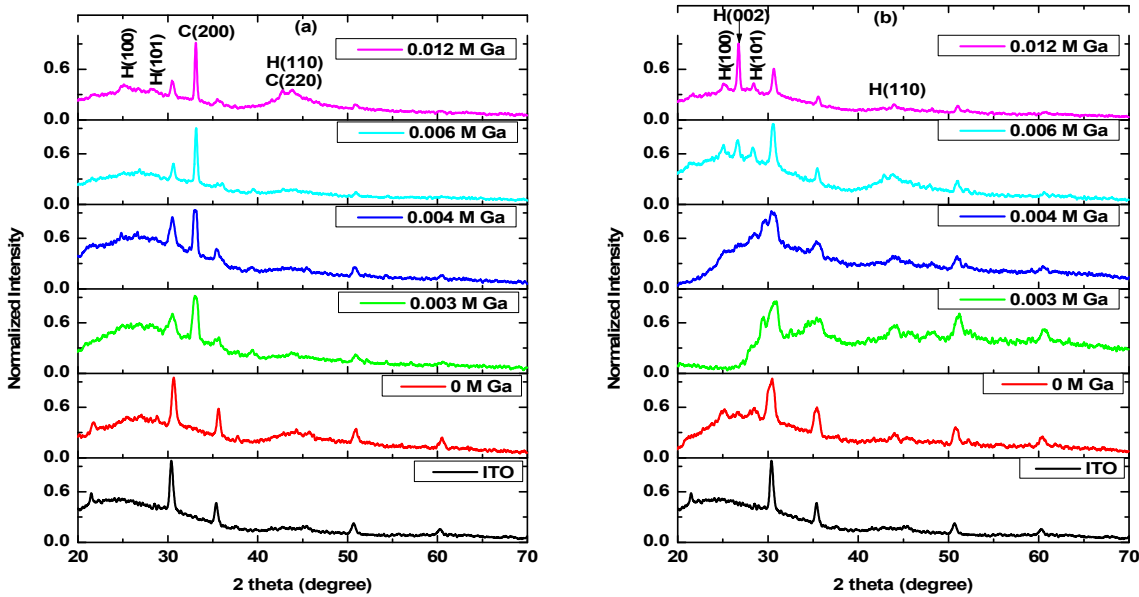

Fig. 2 XRD patterns of (a) as-deposited and (b) annealed un-doped and Ga-doped CdS thin films as a function of Ga concentration in the electrolyte.

The crystallite sizes of the as-deposited CdS:Ga films using the most prominent peak of the cubic phase are in the range (9 - 27) nm, increasing consistently with increase in Ga concentration. It should be noted here however, that any peak broadening due to instrument and

strain effects were neglected in the estimation of these crystallite sizes. The results of analysis of the most prominent cubic (200) peak are presented in Table 1. The Table shows that the structural parameters obtained are very close to those in the JCPDS reference file mentioned above. The lattice constant (a) and inter-planar spacing (d) both slowly decrease below the standard values as Ga concentration increases in the deposition electrolyte, indicating a reduction in the unit cell volume of the crystal. Ga has a smaller ionic radius of 0.62 Å compared to Cd with ionic radius of 0.95 Å while both elements have comparable atomic radii (1.53 Å for Ga and 1.52 Å for Cd). Therefore, a possible replacement of Cd^{2+} by Ga^{3+} in CdS, will likely result in the observed reduction in the lattice parameters, as well as in improvement of the n-type conductivity of CdS. This also suggests that Ga incorporation into CdS took place substitutionally. The fact that there are no observed diffraction peaks belonging to interstitial Ga supports this argument.

Table 1 Structural parameters of (200) peak of the cubic phase of as-deposited CdS:Ga samples with mixed cubic and hexagonal phases.

Ga conc (M)	2θ (°) Ref = 32.78°	FWHM (°)	D (nm)	d (Å) Ref = 2.73 Å	Lattice constant (Å) Ref: a = 5.45 (Å)
0.000	-	-	-	-	-
0.003	33.02	0.9150	9	2.71	5.42
0.004	32.99	0.6392	13	2.71	5.42
0.006	33.14	0.3778	22	2.70	5.40
0.012	33.12	0.3088	27	2.70	5.40

Reference JCPDS file for cubic CdS: 00-021-0829

After annealing, fig. 2 (b) shows that the cubic CdS phase eventually gives way to the hexagonal phase in a thermally-induced re-crystallization process. Only the diffraction peaks belonging to the hexagonal CdS are present in the diffraction patterns. It should be noted at this point that the presence of mixed cubic and hexagonal phases in as-deposited CdS and transformation to pure hexagonal phase after annealing is well-known for CdS electrodeposited using cadmium chloride precursor, FTO substrate and under the conditions similar to the ones used in the present work [17, 30, 31]. The characteristic peaks of the hexagonal phase emerge gradually as Ga concentration increases, with the clearest features at a Ga concentration of 0.012 M. The resulting hexagonal CdS phase now has the preferential orientation of its crystallites in the (002) crystal plane. The results of evaluation of the structural parameters based on this peak are presented in Table 2.

Table 2 Structural parameters of annealed un-doped and Ga-doped CdS samples with pure hexagonal phase. The (002) peak is used for the analysis.

Ga conc (M)	2θ (°) Ref = 26.49°	FWHM (°)	D (nm)	d (Å) Ref = 3.36 Å	Lattice constant (Å)	
					Ref : $a=b$=4.14 Å	Ref: c=6.72 Å
0.000	26.65	1.6544	5	3.34	4.09	6.68
0.003	-	-	-	-	-	-
0.004	26.69	1.5374	5	3.34	4.07	6.67
0.006	26.72	1.1865	7	3.33	4.09	6.66
0.012	26.79	0.3718	22	3.32	4.07	6.65

Reference JCPDS file for hexagonal CdS: 01-075-1545

The results show in the first place, that the lattice parameters are comparable with those of the earlier mentioned reference file. Again, all the lattice parameters ($a = b$, c and d) are smaller in value compared to those of the reference file, while the 2θ values are rather higher than those of the reference file. There is no definite trend in the variation of lattice constants $a = b$ with Ga concentration. However, the lattice parameter (c) and inter-planar spacing (d) both decrease gradually as Ga concentration increases. Again, these results support the substitutional incorporation of Ga into Cd site in the CdS lattice. The obtained crystallite sizes for the un-doped and Ga-doped hexagonal CdS are all smaller than the corresponding values in the cubic phase, and range from 5 nm to 22 nm. They also increase gradually as concentration of Ga in the deposition electrolyte increases.

Figure 3 shows the optical absorbance of (a) as-deposited CdS:Ga and (b) annealed CdS:Ga films with different Ga concentrations from 0.0 M to 0.012 M. Fig. 3 shows that the presence of GaCl$_3$ in the deposition electrolyte and therefore incorporation of Ga into CdS results in increase in absorbance of the resulting CdS films. For the as-deposited films, there is a substantial increase in absorbance of the Ga-doped CdS in the wavelength range greater than the CdS absorption cutoff wavelength (i.e > 500 nm). This increased absorption tail in the long wavelength region is attributed to the presence of significant amount of scattering centers in the as-deposited films as a result of the incorporation of Ga as well as the presence of mixed phases of cubic and hexagonal structures. Therefore fig. 3 (a) shows higher absorbance for all the Ga-doped films compared to the un-doped one. This indicates that the doped film have relatively higher thicknesses arising from higher deposition rate as a result of the presence of Ga in the electrolytic bath and the subsequent incorporation of Ga in the films. Fig. 3(a) also shows a steady increase in absorbance as Ga concentration increases. Fig. 3 (b) generally shows a reduction in absorbance across the entire wavelength range for the Ga-doped samples, although the un-doped sample shows a slight increase in absorbance near 300 nm wavelength. The significant reduction in absorbance is attributed to reduction in scattering centers and presence of single phase (hexagonal) occasioned by re-crystallization on annealing. Again, as in the as-deposited films, the spectra show a general increase in absorbance as Ga concentration in the

electrolytic bath increases. The absorption edges become more clearly defined for all the films after annealing.
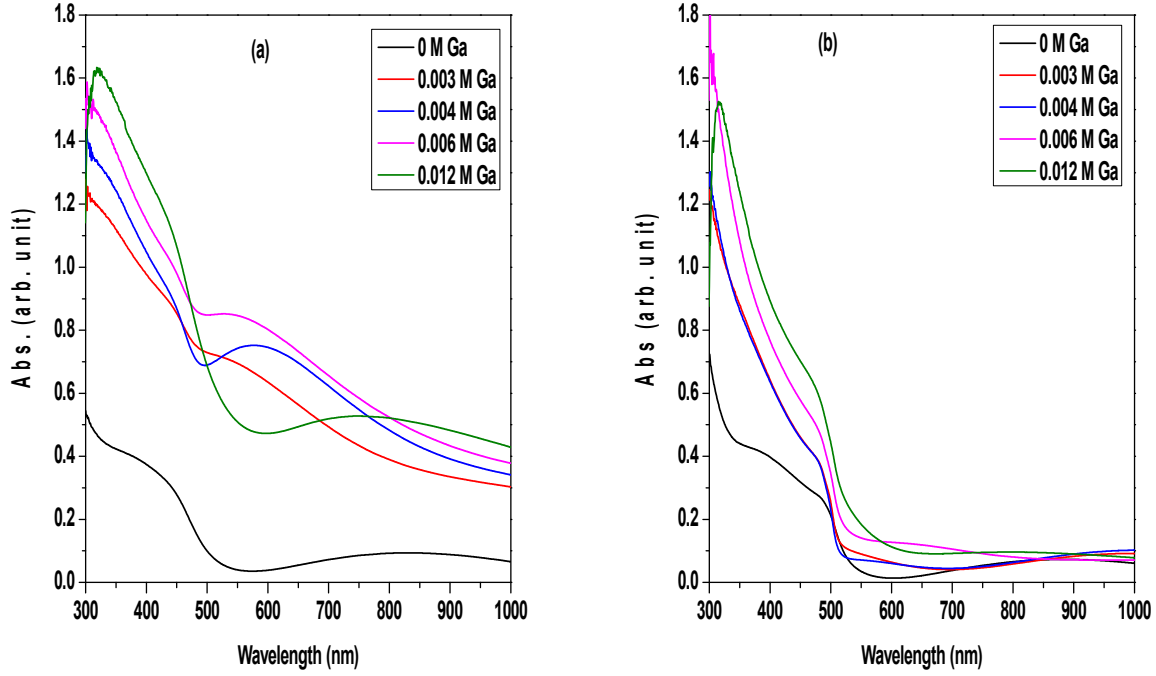

Fig. 3 Optical absorbance of (a) as-deposited and (b) annealed CdS:Ga films as a function of electrolytic Ga concentration.

Figure 4 shows the graphs of square of absorbance vs. photon energy for the estimation of energy bandgap of the CdS films. This is a very convenient and easy way of estimating energy bandgap of semiconductors without actually plotting $(\alpha h\nu)^2$ vs. hν, which requires determination of the thickness of the films and calculating absorption coefficient. The results obtained with this plot are comparable with those obtained from the actual Tauc plot involving $(\alpha h\nu)^2$ vs. hν, where hν is the photon energy [30 - 32]. The absorption edges of the as-deposited CdS:Ga films in fig. 4(a) are not very well defined compared to those of the annealed films (fig. 4 (b)) as mentioned earlier. However, extrapolation of the straight line portion of the graphs immediately after the absorption edges, to the photon energy axis, gives the energy bandgaps of the films. Fig. 4 (a) and (b) both show the absorption of the films to follow the concentration of Ga in the deposition electrolyte, just as was seen in fig. 3. That is to say that the absorption increases as Ga concentration increases. The energy bandgap values estimated from fig. 4 (a) and (b) for both as-deposited and annealed films as a function of Ga concentration in the electrolyte are presented in fig. 5. The error in the bandgap measurement is ±0.02 eV. In as-deposited form, the energy bandgap of the Ga-doped films are generally smaller than that of the un-doped film, with the un-doped film showing a bandgap value of about 2.50 eV.
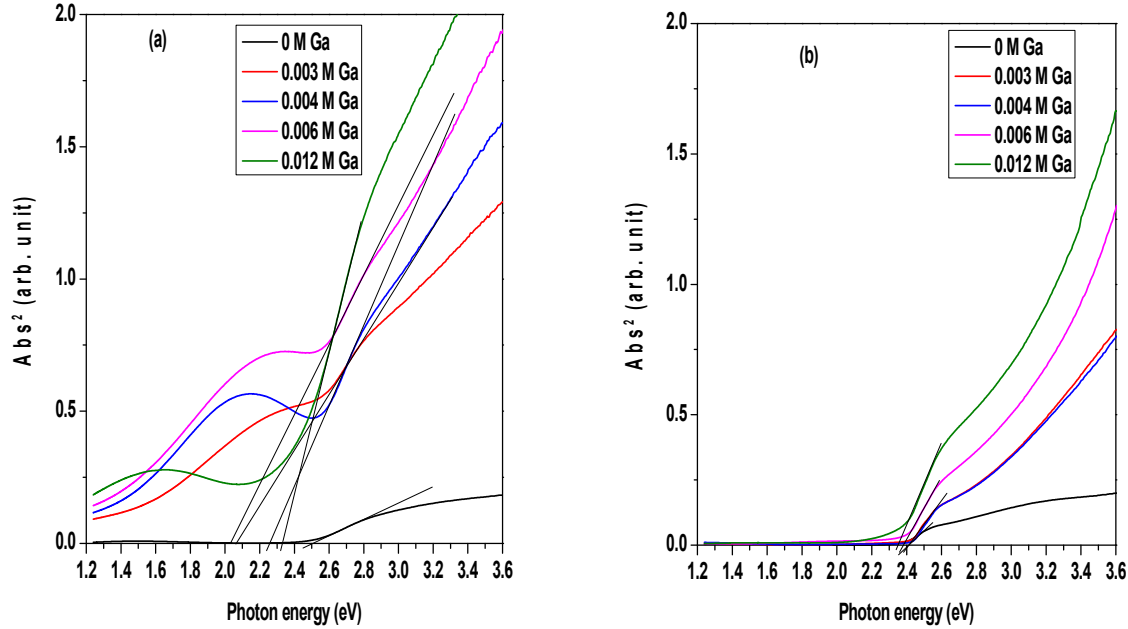
Fig. 4 Graph of square of absorbance vs. photon energy for (a) as-deposited and (b) annealed CdS:Ga films as a function of Ga concentrations in the electrolytic bath.

The values for the doped films are in the range (2.04 – 2.32) eV, with specific values of 2.25 eV, 2.08 eV, 2.04 eV and 2.32 eV for films with Ga concentrations of 0.003 M, 0.004 M, 0.006 M and 0.012 M, respectively. These values gradually decrease as Ga concentration increases up to 0.006 M and then begin to increase for Ga concentration of 0.012 M.

After annealing, fig. 5 shows that there is a reduction in the bandgap of the un-doped film from 2.50 eV to around 2.38 eV, while there is a general increase in the values for the doped samples, with a considerable narrowing of the range to (2.36 – 2.43) eV. The specific values become 2.42 eV, 2.43 eV, 2.39 eV and 2.36 eV for 0.003 M, 0.004 M, 0.006 M and 0.012 M Ga concentrations, respectively. The bandgap gradually increases with Ga concentration up to Ga concentration of 0.004 M, and then gradually decreases beyond this limit to attend the lowest value of 2.36 eV with Ga concentration of 0.012 M. The highest bandgap of 2.43 eV corresponds to Ga concentration of 0.004 M. This is followed by a value of 2.42 eV for Ga concentration of 0.003 M. These two bandgap values are roughly equal to the bulk bandgap of CdS, which is generally taken to be 2.42 eV. Since the best CdS films are obtained after post-deposition annealing, it can be said that the incorporation of Ga into CdS films leads to increase in bandgap, making the Ga-doped materials more beneficial in photovoltaic application as a window/buffer material.
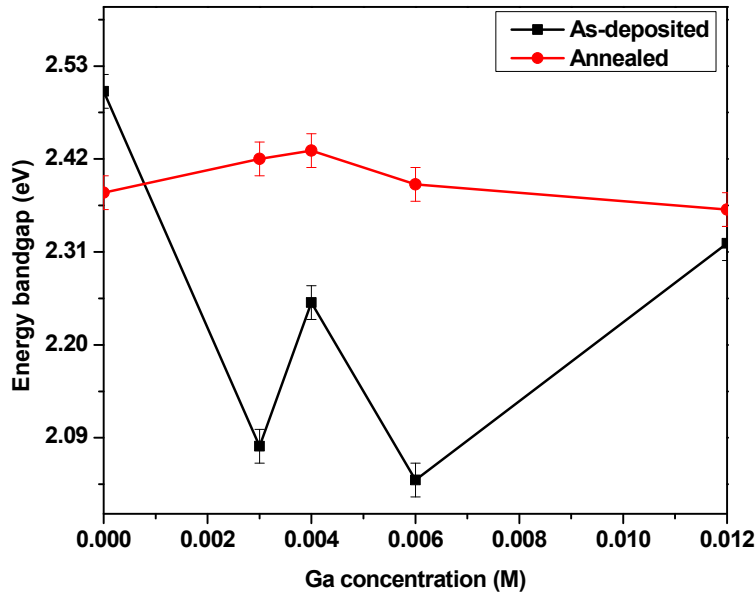
Fig. 5 Energy bandgaps of as-deposited and annealed CdS:Ga as a function of Ga concentration in the electrolytic bath.

This is expected to improve the photocurrent generation of the solar cell, and therefore the short-circuit current density and in turn the conversion efficiency. It is important here to note that the energy bandgap values reported here appear to be under-estimated because of the glass/ITO substrate used. For example, we have repeatedly reported a bandgap value of about 2.42 eV after annealing for un-doped CdS grown on glass/FTO substrate using similar conditions as reported in the present work [17, 30, 33], as against the value of 2.38 eV in the present work. We however attribute this relatively lower bandgap value to the effect of the ITO substrate on these films. Similar results due to the effect of substrate have been reported by other researchers [34] in which they have reported similar lower bandgap of un-doped CdS (even lower than we have reported) on ITO and wider bandgap (similar to what we have reported earlier) on FTO. We have also recently demonstrated the significant effect of TCO substrates on fully fabricated CdS/CdTe solar cells [35]. We therefore attribute the lower bandgap (2.38 eV) of un-doped CdS in the present work to the effect of the ITO substrate used. This effect is also evident in the amorphous XRD pattern of this un-doped film as we have seen earlier, and very smooth (with no visible grains) SEM image of this same sample, as we shall see in the discussion on SEM result, as compared to that of CdS on FTO as we have reported previously in refs [17, 30, 33]. Based on the above, the increase in bandgap we are reporting for Ga-doped CdS films is with respect to the un-doped CdS in the present work. We therefore believe that if this work is repeated using FTO substrate, the improvement in bandgap with respect to un-doped CdS will still be clearly evident. It may also be necessary to note that other workers [23, 24, 25] before us have generally reported

decreased energy bandgap with Ga doping and generally lower bandgap for both un-doped and Ga-doped CdS in the range (2.12 eV - 2.32 eV) using other techniques, with only one group [23] reporting bandgap of 2.41 eV for un-doped CdS. In the present work, we are reporting improvement in bandgap with Ga doping using electrodeposition technique.

This observed bandgap increase as a result of incorporation of Ga dopants (with up to 0.006 M Ga concentration in the electrolyte) can be explained by the well-documented Burstein-Moss effect which is increase in energy bandgap as a result of band filling, whereby increased n-type doping of a semiconductor results in electrons from the dopant atoms occupying/filling the lowest energy levels near the bottom of the conduction band. This results in the Fermi level moving into the conduction band above these occupied energy levels. Thus, optical transition involves higher empty band states in the conduction band, resulting in a blueshift of the fundamental absorption edge. This phenomenon is said to be made possible due to the low effective mass of the conduction band electrons [36, 37]. This was first observed in InSb [36, 37] and has also been reported for In-doped CdS [38].

The gradual bandgap reduction for higher Ga concentrations of 0.006 M and 0.012 M can also be explained to be as a result of bandgap renormalization [39]. This phenomenon is said to be as a result of mutual exchange and Coulomb interaction between the excess free electrons in the conduction band and electron-ionized impurity scattering, which causes a decrease in the energy of the conduction band minimum (in the case of n-type doping) and an increase in the energy of the valence band maximum (in the case of p-type doping) [39].

Figure 6 shows the optical transmittance of the un-doped and doped CdS films in both as-deposited and annealed forms. The as-deposited and Ga-doped films in fig. 6 (a) show very poor transmittance compared to the un-doped film. This is attributed to high density of scattering centers in these materials as a result of Ga incorporation. The transmittance tends to decrease as Ga concentration in the electrolyte increases. After annealing, however, fig. 6 (b) shows a drastic improvement in transmittance especially for the Ga-doped films, indicating a substantial reduction in the scattering centers. The transmittance also roughly follows the Ga concentration, slightly decreasing as Ga concentration in the electrolyte increases, with the un-doped film having the highest transmittance. In any case, the transmittance levels observed for both doped and un-doped films are significantly high enough for solar cell application even at the long deposition time of 45 minutes used (indicating considerably high thickness). As mentioned earlier in the experimental details section, these transmittance values can still be improved significantly by reducing the deposition time to few minutes which will also have the effect of reducing the film thickness. In addition, the slight improvement in energy bandgap over the un-doped film, for moderately doped films will help to balance the effect of the slight decrease in transmittance for doped films.
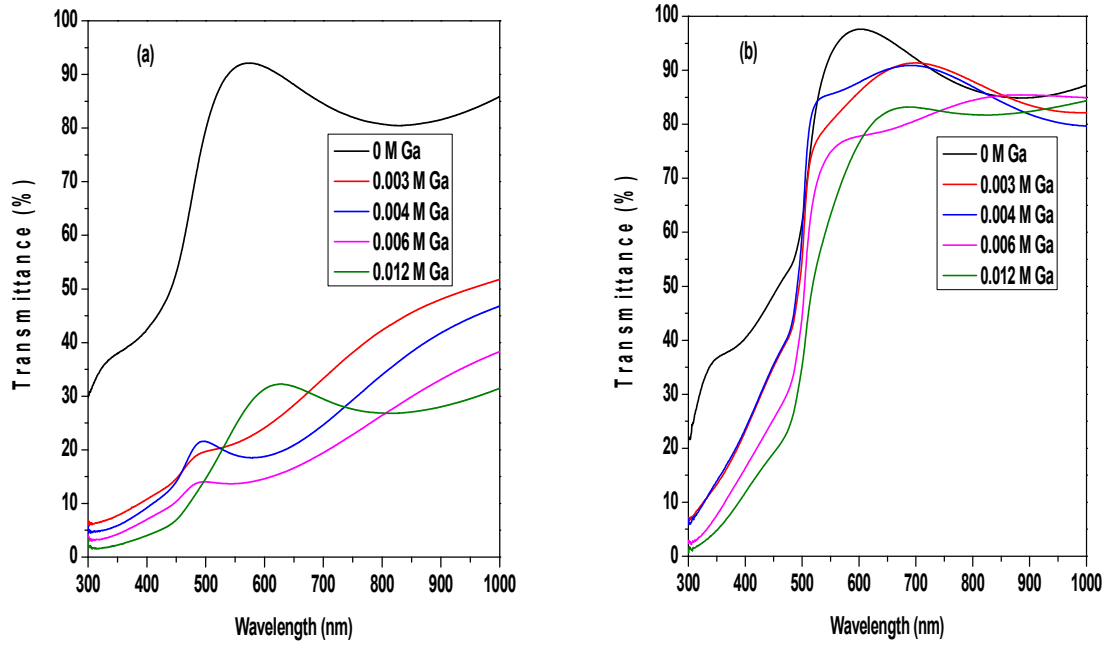
Fig. 6 Optical transmittance of un-doped and Ga-doped CdS in (a) as-deposited and (b) annealed forms, as a function of Ga concentration in the electrolytic bath.

Figure 7 shows the room temperature photoluminescence spectra of the annealed CdS:Ga films as a function of Ga concentration in the deposition electrolytic bath. The PL spectra were recorded in the wavelength range of 400 nm – 600 nm, using an excitation wavelength of 338 nm. All doped and un-doped CdS films show a single PL peak in the wavelength range of (519 – 526) nm, corresponding to the green emission, with all the Ga-doped films generally having their peak centers shifted towards lower wavelengths below that of the un-doped film (which is 526 nm). Again, the peak intensities generally increase as Ga concentration increases, indicating an improvement in the green emission for possible light emitting diode application. This observed general trend suggests that the amount of Ga incorporated into the CdS is in fairly direct proportionality with the concentration of Ga in the deposition electrolytic bath. A summary of the PL peak analysis is presented in Table 3.
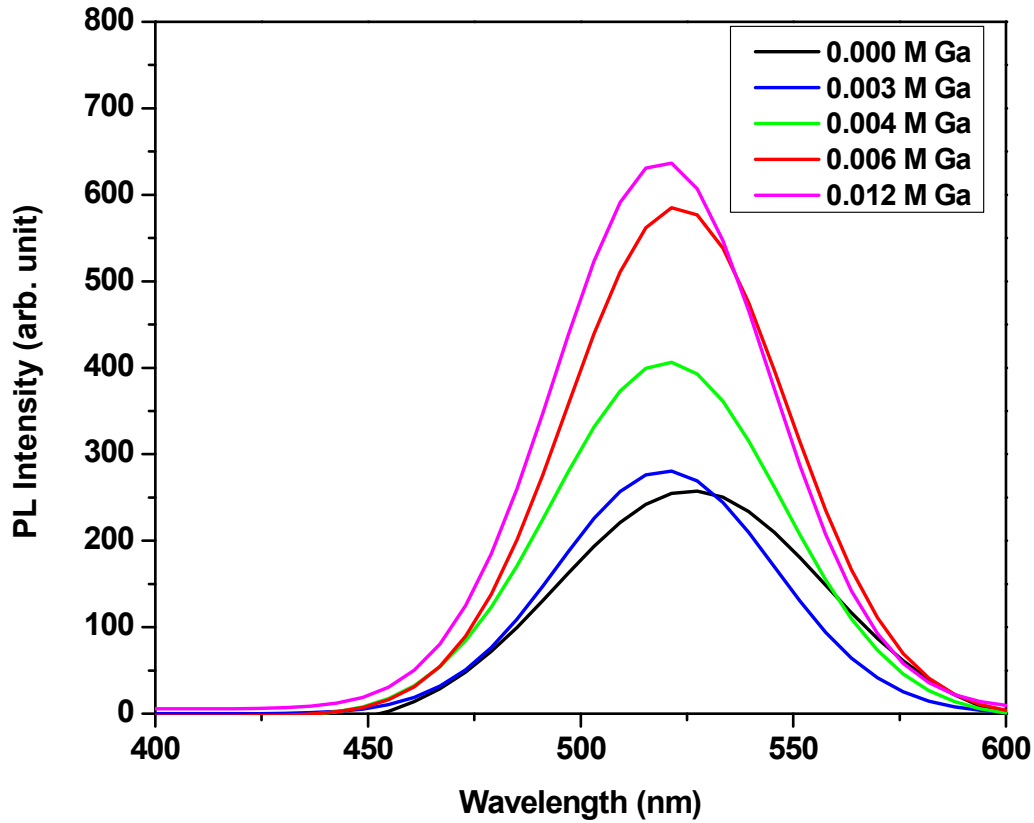
Fig. 7 Room temperature photoluminescence spectra of the annealed un-doped and doped CdS films with different concentrations of Ga in the deposition electrolyte.

A close look at Table 3 shows that the peaks of all the Ga-doped CdS become narrower compared to the un-doped sample, as can be seen from the FWHM values. Also the shifting of the peak centers of Ga-doped films towards lower photon wavelength produces a blueshift in the corresponding peak centre energy. This is also in agreement with the trend of energy gap obtained from the absorption curve in figs. 4 and 5, where the bandgaps of the doped films are generally higher than that of un-doped film up to Ga concentration of 0.006 M. It should be noted that a comparison of the trend in energy bandgap and PL peak energy of Ga-doped CdS in the present work and those reported by previous researchers are opposite. Whereas the present work shows blueshift in these values, Cai *et al*. obtained a redshift of PL peaks in their Ga-doped CdS nanowires grown by thermal evaporation with Ga concentrations in the range 1%, 2%, 4% and 8%, thus indicating a narrowing of bandgap with Ga incorporation [26]. Khallaf *et al*. also reported bandgap narrowing of their Ga-doped CBD-grown CdS thin films [23]. In the same

vein, Yang *et al*. reported bandgap shrinkage in their Ga-doped CdS powder grown by the solvothermal method [25].

Table 3 Summary of PL peaks analysis and energy bandgap (from optical absorption) of annealed CdS:Ga films as a function of Ga concentrations in the deposition bath.

Ga conc. (M)	Peak centre wavelength (nm)	Peak center energy (eV)	Peak intensity (arb. unit)	FWHM (nm)	E_g from optical absorption (eV)
0.000	526	2.36	260	74	2.38
0.003	520	2.38	281	60	2.42
0.004	520	2.38	406	64	2.43
0.006	523	2.37	585	61	2.39
0.012	519	2.39	636	60	2.36

Figure 8 shows the representative energy dispersive X-ray spectrum for CdS:Ga thin films. All the CdS:Ga films have similar EDX spectra, and for this reason as well as to save journal page, only one representative spectrum is presented here. The spectrum clearly shows the presence of all three elements of interest (Cd, S and Ga). The percentage atomic composition of all the CdS and CdS:Ga films in both as-deposited and annealed forms are summarized in Table 4.
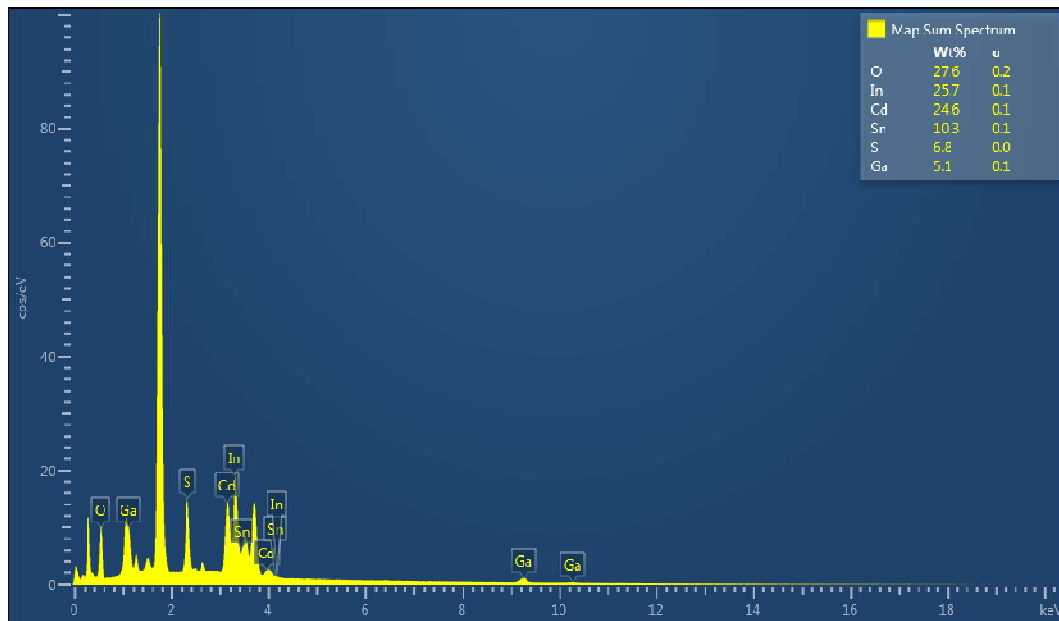

Fig. 8 Typical EDX spectrum of CdS:Ga films.

Table 4 Percentage atomic composition of CdS:Ga films grown with different Ga concentrations

Ga conc (M)	Percentage atomic composition (±0.1%)					
	As-deposited			Annealed		
	Cd	S	Ga	Cd	S	Ga
0	54.5	45.5	0.0	55.4	44.6	0.0
0.003	47.6	43.8	8.6	48.4	44.8	6.8
0.004	46.1	41.5	12.4	46.5	43.5	10.0
0.006	43.6	41.8	14.6	44.3	42.2	13.5
0.012	43.8	42.9	13.3	43.6	41.6	14.8

In as-deposited form, all the films are Cd-rich with Cd and S atomic compositions fairly decreasing as Ga concentration in the electrolyte increases, as shown in fig. 9 (a). On the other hand, the atomic concentration of Ga fairly increases as molar concentration of Ga in the electrolyte increases as shown in fig. 10. The slight distortion in these trends for Ga concentrations of 0.006 M and 0.012 M is attributed to non-homogeneity of the films (as well as presence of mixed phases) in as-deposited form. To certain extent, electrodeposited materials are known to show their best quality after post-deposition annealing process, which ensures homogeneity of the materials as a result of thermally-induced re-crystallization. This is partly because these materials are grown at relatively low temperature, compared to materials grown by other advanced techniques under vacuum condition.

In annealed form, Table 4 and fig. 9 (b) also show that percentage atomic compositions of both Cd and S decrease as molar concentration of Ga in the electrolyte increases, with a slight deviation in the case of S for the sample grown with 0.003 M Ga. The materials are again Cd-rich in general. In the case of atomic percentage of Ga, there is a continuous increase as molar concentration of Ga in the electrolyte increases as shown in fig. 10. There is therefore a clear direct relationship between the molar concentration of Ga precursor in the deposition electrolyte and the actual amount of Ga atoms incorporated into the deposited films. Fig. 10 also shows that there is a general decrease in the percentage atomic Ga composition in the films after annealing except for the film grown with 0.012 M Ga concentration, in which case the percentage atomic concentration of Ga is higher in the annealed film than in the as-deposited one. Although EDX is not a very precise technique for quantitative analysis of chemical composition of these films, it however provides a qualitative insight into the composition of these materials.
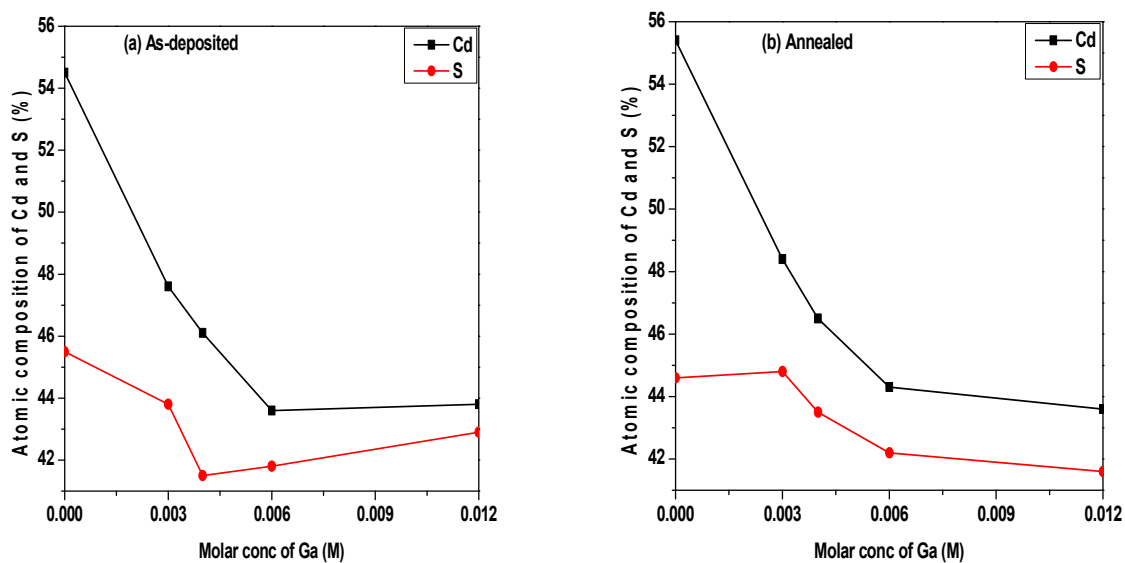
Fig. 9 Percentage atomic concentration of Cd and S in (a) as-deposited and (b) annealed CdS:Ga films, as a function of molar concentration of Ga in the deposition electrolyte.
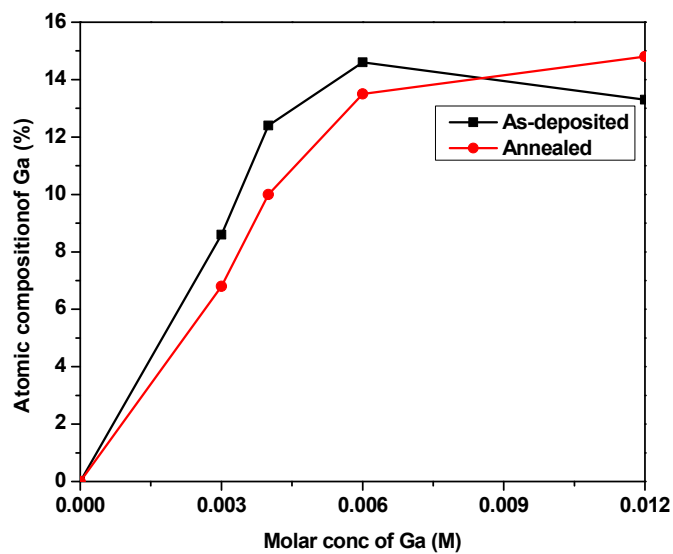

Fig. 10 Percentage atomic cocentration of Ga in as-deposited and annealed CdS:Ga films as a function of molar concentration of Ga in the deposition electrolyte.
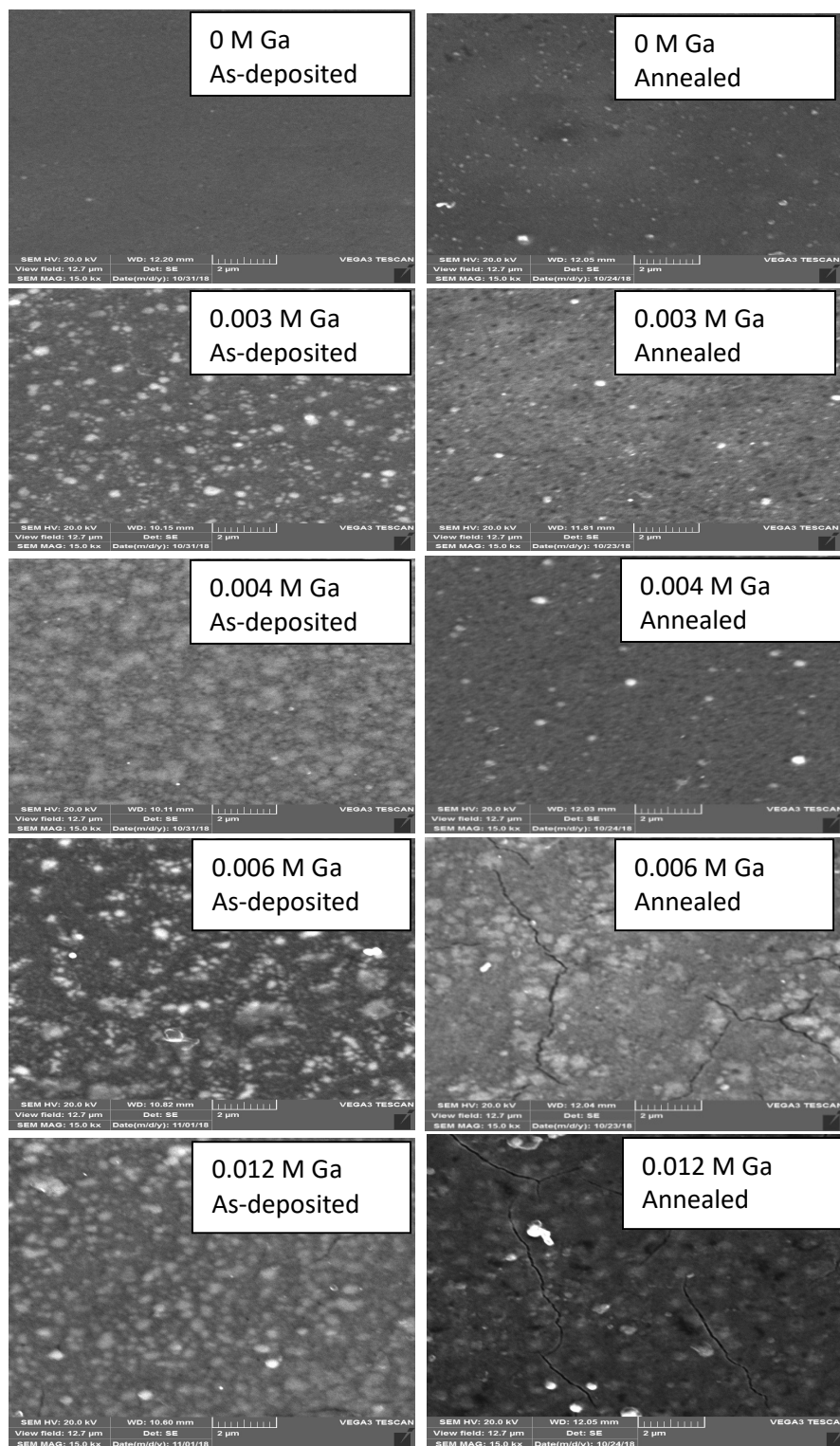
Fig. 11 SEM images of as-deposited and annealed CdS:Ga grown with different Ga concentrations in the electrolyte.

Figure 11 shows the surface SEM images of the un-doped and Ga-doped CdS films in both as-deposited and annealed forms. The image of the un-doped film in as-deposited form shows a highly uniform, dense and pinhole/crack-free deposit with no visible grains. It can be recalled that XRD of this same sample shows it to be amorphous or weakly crystalline, thus corroborating this observed smooth surface without visible grains. After annealing, fig. 11 shows that the film gradually begins to show evidence of grain size distribution. With the incorporation of Ga into the films, the rest of the images show clear indication of grains although the sizes of these grains are difficult to estimate. After post-deposition annealing, the surfaces of the films appear to be smoother. However, as the Ga-content of the deposition electrolyte increases beyond 0.004 M, the film surfaces begin to show very visible cracks, indicating two possibilities. One possibility is that Ga concentration beyond 0.004 M in the deposition bath is not helpful in producing films with crack-free surfaces. The second possibility is that the annealing conditions applied to these films (400 °C for 20 minutes) are not favorable to the films beyond 0.004 M of Ga concentration. Between these two situations, the more probable case seems to be the first as the cracks are not observed in all the annealed films.

This situation has severe implications in device application such as in solar cell fabrication. In this case, the cracks will provide unwanted shunting paths when these films are used as window/buffer layers. This will have direct negative impact on the open-circuit voltage and fill factor and therefore resulting in very poor cell efficiency. To avoid this adverse effect, there are two possibilities. One is not to have more than 0.004 M Ga in the deposition bath. Next is to grow the films for few minutes so that very small amount of Ga gets incorporated into the films, as the amount of Ga incorporated into the film is also a function of deposition time.

4 Conclusion

Ga-doping of CdS thin films has been effectively achieved using the electrodeposition method, with glass/ITO as substrate and $GaCl_3$ as source of Ga ions, for the first time. The increase in the concentration of $GaCl_3$ in the deposition electrolyte from 0.0 M to 0.012 M, results in increase in the amount of Ga atoms incorporated into the deposited CdS films. XRD results show that the incorporation of Ga into the CdS films helps in the crystallization of the films. The CdS:Ga films crystallize in mixed cubic and hexagonal phases in as-deposited form, under the conditions used, but transform into the pure hexagonal crystal phase after post-deposition annealing. Optical characterization shows that incorporating Ga into CdS films slightly increases the energy bandgap of the CdS relative to the un-doped sample in accordance with the Burstein-Moss effect, therefore making these films advantageous for application as window/buffer layers in solar cells. Room temperature PL measurements of all the doped and un-doped films show only a single green light emission peak with peak centre energy values supporting the Burstein-Moss effect in the doped films. Results of SEM imaging of the film surfaces indicate that Ga incorporation with $GaCl_3$ concentrations above 0.004 M may not be suitable for device application due to the

existence of cracks in the films. This work goes a long way to showing one of the strengths of the electrodeposition technique (i.e. the ease of doping) as a semiconductor growth technique for device application. Further work on this project will be geared towards optimization of the growth and processing conditions as well as incorporation of these films into CdTe-based solar cells in order to fully explore their potentials.

Conflict of interest

Authors declare no conflict of interest.

References

[1] W. Wondmagegn, I. Mejia , A. Salas-Villasenor , H. J. Stiegler, M. A. Quevedo-Lopez, R. J. Pieper, B. E. Gnade, CdS thin film transistor for inverter and operational amplifier circuit Applications. Microelectron. Eng. **157**, 64–70 (2016).

[2] T. Gaewdang, N. Wongcharoen, Heterojunction properties of p-CuO/n-CdS Diode. Adv. Mater. Res. **1098**, 1 – 5 (2015).

[3] Y. Kraftmankher, Experiments on photoconductivity. Eur. J. Phys. **33**, 503 – 511 (2012).

[4] X. Wang, X. He, H. Zhu, L. Sun, W. Fu, X. Wang, L. C. Hoong, H. Wang, Q. Zeng, W. Zhao, J. Wei, Z. Jin, Z. Shen, J. Liu, T. Zhang, Z. Liu, Subatomic deformation driven by vertical piezoelectricity from CdS ultrathin films. Sci. Adv. **2** (7), 1-9 (2016).

[5] A. K. Bansal, F. Antolini, S. Zhang, L. Stroea, L. Ortolani, M. Lanzi, E. Serra, S. Allard, U. Scherf, I. D. W. Samuel, Highly luminescent colloidal CdS quantum dots with efficient near-infrared electroluminescence in light-emitting diodes. J. Phys. Chem. C **120**, 1871−1880 (2016).

[6] S. K. Tripathi, R. K. Jyoti, Investigation of non-linear optical properties of CdS/PS polymer nanocomposite synthesized by chemical route. Opt. Commun. **352**, 55–62 (2015).

[7] A. A. Ojo, I. M. Dharmadasa, Optimisation of pH of cadmium chloride post-growth-treatment in processing CdS/CdTe based thin film solar cells. J. Mater. Sci: Mater. Electron. **28**,7231–7242 (2017).

[8] J. Schaffner, E. Feldmeier, A. Swirschuk, H. J. Schimper, A. Klein, W. Jaegermann, Influence of substrate temperature, growth rate and TCO substrate on the properties of CSS-deposited CdS thin films. Thin Solid Films **519**, 7556 – 7559 (2011).

[9] N. Memarian, S. M. Rozati, I. Concina, A. Vomiero, Deposition of Nanostructured CdS

thin films by thermal evaporation method: Effect of substrate temperature. Materials **10**, 773 (2017); doi:10.3390/ma10070773.

[10] N. R. Paudel, K. A. Wieland, A. D. Compaan, Ultrathin CdS/CdTe solar cells by Sputtering. Sol. Energ. Mater. Sol. Cell. **105**, 109 – 112 (2012).

[11] A. H. Rubel, J. Podder, Optical properties of spray pyrolysis deposited CdS:Al thin Films. Journal of Bangladesh Academy of Sciences **39** (1), 25 - 30 (2015).

[12] T. Aramoto, S. Kumazawa, H. Higuchi, T. Arita, S. Shibutani, T. Nishio, J. Nakajima, M. Tsuji, A. Hanafusa, T. Hibino, K. Omura, H. Ohyama, M. Murozono, 16.0% Efficient Thin-Film CdS/CdTe Solar Cells. Jap. J. Appl. Phys. **36**, 6304 – 6305 (1997).

[13] J. Avila-Avendano, I. Mejia, H. N. Alshareef, Z. Guo, C. Young, M. Quevedo-Lopez, In-situ CdS/CdTe heterojuntions deposited by pulsed laser deposition. Thin Solid Films **608**, 1– 7 (2016).

[14] P. Boieriu, R. Sporken, Y. Xin, N. D. Browning, S. Sivananthan, Wurtzite CdS on CdTe grown by molecular beam epitaxy, J. Electron. Mater. **29** (6), 718-722 (2000).

[15] A. A. Ziabari, F. E. Ghodsi, Growth, characterization and studying of sol-gel derived CdS nanocrystalline thin films incorporated in polyethyleneglycol: Effect of post-growth heat treatment. Sol. Energ. Mater. Sol. Cell. **105**, 249 – 262 (2012).

[16] Z. Lu, R. Jin, Y. Liu, L. Guo, X. Liu, J. Liu, K. Cheng, Z. Du, Optimization of chemical bath deposited cadmium sulfide buffer layer for high-efficient CIGS thin film solar cells. Mater. Lett., **204**, 53–56 (2017).

[17] O. K. Echendu, F. B. Dejene, I. M. Dharmadasa, F. C. Eze, Characteristics of Nanocrystallite-CdS produced by low-cost electrochemical technique for thin film photovoltaic application: The influence of deposition voltage. Int. J. Photoenerg. Volume 2017, Article ID 3989432, 13 pages https://doi.org/10.1155/2017/3989432.

[18] M. Kim, A. Ochirbat, H. J. Lee, CuS/CdS quantum dot composite sensitizer and its applications to various TiO$_2$ mesoporous film-based solar cell devices. Langmuir **31**, 7609−7615 (2015).

[19] N. Naghavi, G. Renou, V. Bockelee, F. Donsanti, P. Genevee, M. Jubault, J. F. Guillemoles, D. Lincot, Chemical deposition methods for Cd-free buffer layers in CI(G)S solar cells: Role of window layers. Thin Solid Films **519**, (21) 7600 – 7605 (2011).

[20] H. Cui, X. Liu, L. Sun, F. Liu, C. Yan, X. Hao, Fabrication of efficient Cu$_2$ZnSnS$_4$ solar cells by sputtering single stoichiometric target. Coatings **7**, 19 (2017); doi:10.3390/coatings7020019.

[21] O. K. Echendu, F. Fauzi, A. R. Weerasinghe, I. M. Dharmadasa, High short-circuit current density CdTe solar cells using all-electrodeposited semiconductors. Thin Solid Films **556**, 529 – 534 (2014).

[22] J. H. Lee, J. S. Yi, K. J. Yang, J. H. Park, R. D. Oh, Electrical and optical properties of boron doped CdS thin films prepared by chemical bath deposition. Thin Solid Films **431 – 432**, 344–348 (2003).

[23] H. Khallaf, G. Chai, O. Lupan, L. Chow, S. Park, A. Schulte, Characterization of

gallium-doped CdS thin films grown by chemical bath deposition, Appl. Surf. Sci. **255** 4129–4134 (2009)

[24] S. Alhammadi, H. Jung. S. Kwon. H. Park. J. J. Shim, M. H. Cho, M. Lee, J. S. Kim, W. K. Kim, Effect of gallioun doping on CdS thin film properties and corresponding Cu(InGa)Se$_2$/CdS:Ga solar cell performance. Thin Solid Films 2018 (In press); doi:10.1016/j.tsf.2018.06.014.

[25] J. Yang, R. Liu, S. Huang, Y. Shao, Y. Huang, Y. Yu, Enhanced photocatalytic activity and stability of interstitial Ga-doped CdS: Combination of experiment and calculation. Catalysis Today **224** (2014) 104–113

[26] J. Cai, J.Jie, P. Jiang, D. Wu, C. Xie, C. Wu, Z. Wang, Y. Yu, L. Wang, X. Zhang, Q. Peng, Y. Jiang, Tuning the electrical transport properties of n-type CdS nanowires via Ga doping and their nano-optoelectronic applications. Phys. Chem. Chem. Phys. **13**, 14663–14667 (2011).

[27] O. K. Echendu, I. M. Dharmadasa, Graded-Bandgap solar cells using all-electrodeposited ZnS, CdS and CdTe thin-films. Energies **8**, 4416 – 4435 (2015): doi:10.3390/en8054416.

[28] R. N. Bhattacharya. CIGS-based solar cells prepared from electrodeposited stacked Cu/In/Ga layers. Sol. Energ. Mater. Sol. Cell. **113**, 96 – 99 (2013).

[29] J. Tao, L. Chen, H. Cao, C. Zhang, J. Liu, Y. Zhang, L. Huang, J. Jiang, P. Yang, J. Chu, Co–electrodeposited Cu$_2$ZnSnS$_4$ thin–film solar cells with over 7% efficiency fabricated via fine–tuning of the Zn content in absorber layers. J. Mater. Chem. A (2013): DOI: 10.1039/C5TA09636G

[30] O. K. Echendu, U. S. Mbamara, K. B. Okeoma, C. Iroegbu, C. A. Madu, I. C. Ndukwe, I. M. Dharmadasa, Effects of deposition time and post-deposition annealing on the physical and chemical properties of electrodeposited CdS thin films for solar cell application. J. Mater. Sci.: Mater. Electron. **27**, 10180 – 10191 (2016).

[31] N. A. Abdul-Manaf, A. R. Weerasinghe, O. K. Echendu, I. M. Dharmadasa, Electro-plating and characterisation of cadmium sulphide thin films using ammonium thiosulphate as the sulphur source, J. Mater Sci: Mater. Electron. **26**, 2418–2429 (2015).

[32] O.K. Echendu, S.Z. Werta, F.B. Dejene, V. Craciun, Electrochemical deposition and characterization of ZnOS thin films for photovoltaic and photocatalysis applications. J. Alloys Compd. **769**, 201 – 209 (2018).

[33] O. K. Echendu, S. Z. Werta, F. B. Dejene, K. O. Egbo, Structural, vibrational, optical, morphological and compositional properties of CdS films prepared by a low-cost electrochemical technique, J. Alloys Compd. **778**, 197 – 203 (2019).

[34] A. C. S. De Alwis, H. Y. R. Atapattu and D. S. M. De Silva, Influence of the type of conducting glass substrate on the properties of electrodeposited CdS and CdTe thin films, J. Mater. Sci: Mater. Electron. **29** (4), 12419 – 12428 (2018).

[35] O. K. Echendu, F. B. Dejene and I. M. Dharmadasa, An investigation of the influence of different transparent conducting oxide substrates/ front contacts on the performance of CdS/CdTe thin film solar cells, J. Mater. Sci: Mater. Electron. **28**, 18865 – 18872 (2017).

[36] E. Burstein, Anoma1ous optical absorption limit in InSb. Phys. Rev. **93**, 632 – 633 (1954).

[37] T. S. Moss, The interpretation of the properties of indium antimonide. Proc. Phys. Soc. B **67**, 775 (1954).

[38] H. Jager, E. Seipp, Burstein-Moss shift in heavily In-doped evaporated CdS layers, J. Appl. Phys. **52**(1), 425 - 427 (1981).

[39] K. F. Berggren, B. E. Sernelius, Band-gap narrowing in heavily doped many-valley Semiconductors. Phys. Rev. B **24** (4), 1971 – 1986 (1981).